Biointerface Research in Applied Chemistry
Platinum Open Access Journal (ISSN: 2069-5837)

Article
Volume 12, Issue 4, 2022, 4567 - 4583
https://doi.org/10.33263/BRIAC124.45674583

Optimization of Methylene Blue Adsorption on Agricultural Solid Waste Using Box–Behnken Design (BBD) Combined with Response Surface Methodology (RSM) Modeling

Abdellah Dbik [1], Noureddine El Messaoudi [1,*], Safae Bentahar [1], Mohammed El Khomri [1], Abdellah Lacherai [1], Nadia Faska [1,2]

[1] Laboratory of Applied Chemistry and Environment, Faculty of Science, Ibn Zohr University, Agadir 80000, Morocco
[2] Faculty of Applied Sciences, Ibn Zohr University, Ait Melloul 86150, Morocco
* Correspondence: noureddine.elmessaoudi@edu.uiz.ac.ma (N.E), abdellah.dbik@edu.uiz.ac.ma (A.D);
Scopus Author ID 56465946700

Received: 15.08.2021; Revised: 16.09.2021; Accepted: 18.09.2021; Published: 3.10.2021

Abstract: Tunics corm saffron (TCS) is a low-cost adsorbent that removes methylene blue (MB) from an aqueous solution. The TCS was characterized using FTIR and SEM analysis. The influence of MB adsorption variables such as TCS dose (0.4–2.4 g L^{-1}), contact time (0–120 min), MB dye concentration (100–500 mg L^{-1}) was optimized Box–Behnken design (BBD) combined with response surface methodology (RSM) modeling. All three variables among the main parameters significantly affected the removal efficiency by applying the quadratic regression analysis. The results showed that the predicted values for MB adsorption were close to the experimental values and were in good agreement. Besides, the r^2 value (r^2=0.970) indicates that the regression can predict response for the adsorption process in the studied range. The optimum BBD-RSM for MB removal of 89.48 % was recorded at a TCS dose of 1.78 g L^{-1}, contact time of 56 min, MB dye concentration of 176 mg L^{-1} at solution pH of 5.4 temperature 21 °C. Excellent regeneration of TCS to remove MB in sixth consecutive adsorption-desorption cycles. This work highlights that TCS offers tremendous potential as a low-cost for organic dyes removal from wastewaters.

Keywords: methylene blue; adsorption; tunics corm saffron; BBD; RSM.

1. Introduction

With the rapid development of human society, harmful dyes are becoming the primary source of water pollution and represent a significant environmental concern [1]. Dyes are an essential source of water pollution. They are used in many areas such as textile, tannery, paper pulp, cosmetics, plastics, leather, printing, rubber, food, and pharmaceutical industries [2–6]. These dyes are allergic substances, carcinogenic, and toxic for the health of humans and animals, and aquatic life, and the environment [7–12]. Methylene blue, a cationic dye, is a water-soluble dye with high chromaticity, extensively used in chemical indicators, dyes, biological stains, and drugs [13–15]. It is pretty visible and stable in water at room temperature [16].

Adsorption is the most effective method used to remove dyes from aqueous solution compared to other techniques (coagulation, photocatalysis, flocculation, hydrogen peroxide, adsorption, oxidation, irradiation, ion exchange, reverse osmosis, advanced oxidation,

membrane filtration, precipitation) due to their ease of operation, high efficiency, low-energy requiring technology, availability of different adsorbents, effectiveness in regeneration and reuse of the adsorbent [17–22].

In this context, many researchers developed low-cost materials such as agricultural solid wastes to minimize the pollution of wastewaters. Agricultural solid wastes contain main components: cellulose, lignin, hemicelluloses, lipids, proteins, etc. [23,24]. Besides are available and abundant in large quantities and have high potential sorbents due to the variety of functional groups (–OH, –C=O, –C–O, –NH_2) on their surfaces [25,26]. As a result, agricultural solid wastes can be used as an economical and eco-friendly adsorbent since they are abundant and renewable sources [27]. Many agricultural solid wastes are used for the removal of dyes from an aqueous solution, such as date stones (*Phoenix dactylifera*) [28], jujube shells (*Ziziphus lotus*) [29], shell Argan nuts [30], *Clitoria fairchildiana* [31], Olive pomace [32], Leaves of Platanus [33], Walnut shell [34], Jojoba residues [35], *Calotropis procera* [36], Mandarin Peel [37], Banana peel [38], *Eragrostis plana* Nees [39], and waste of *citrus sinesis* [40]. The tunics corm saffron is agricultural solid waste abundant and available in Morocco. The saffron (*Crocus sativus* L.) is used in the food, dairy, dye industries, cooking, medicines, cosmetics, and perfumes [41].

In this study, the tunics corm saffron was used to remove methylene blue from an aqueous solution. The prepared adsorbent was characterized by Fourier transform infrared (FTIR) and scanning electron microscope (SEM) analysis. Furthermore, the fundamental parameters affecting the MB dye adsorption, such as adsorbent dose, contact time, and MB dye concentration, were optimized via Box-Behnken design (BBD) in response surface methodology (RSM). Finally, the regeneration of TCS to remove MB in multiple consecutive adsorption-desorption cycles was studied.

2. Materials and Methods

2.1. Chemicals.

The methylene blue (cationic dye, $C_{16}H_{18}ClN_3S$, CI=52015, MW=319.85 g mol^{-1}, λ_{max}=661 nm) and the hydrochloric acid (HCl) used in this study were purchased from Sigma-Aldrich.

2.2. Preparation and characterization of adsorbent.

Tunics corm saffron (*Crocus sativus* L.) was collected in Taliouine (South of Morocco). The material was washed distilled water and placed in an oven at 90 °C for 24 h, then ground on a laboratory mill and sieved with size 50-100 μm on laboratory sieve. The prepared adsorbent was characterized by Fourier transform infrared (FTIR) spectroscopy with resolution 4 cm^{-1} in a spectrometer Jasco 4100 and coupled with attenuated total reflectance (ATR) technique in the range 4000-500 cm^{-1} was used to determine the functional groups present in their surface, scanning electron microscope (SEM) on SUPRA 40 VP at tension 20 kV was utilized to specify the morphology of TCS.

2.3. Adsorption experiments.

The adsorption experiments were conducted by adding the 0.09 g of TCS to 50 mL of MB dye solutions with a concentration of 100 mg L^{-1} in batch mode. The mixture was agitated

at 150 rpm at 21±1 °C and pH (MB) = 5.4. The influence of different parameters liked as TCS dose (0.4–2.4 g L^{-1}), contact time (0–120 min), MB dye concentration (100–500 mg L^{-1}) on dye adsorption was evaluated. After completing the experiment, the dye solution was filtered through centrifuging at 3500 rpm for 5 min. The concentration of residual MB was measured using a UV/Vis spectrophotometer (2300/Techcomp) at 661 nm as λ_{max} . The quantity absorbed q_e (mg g^{-1}), and removal efficiency (%) of MB on TCS were calculated by the equations given below:

$$q_e = \frac{(C_0 - C_e) \times V}{W} \quad (1)$$

$$\%\ Removal = \frac{(C_0 - C_e)}{C_0} \times 100 \quad (2)$$

where C_0 (mg L^{-1}) and C_e (mg L^{-1}) are the MB concentrations before and after adsorption, respectively, V (L) is the dye solution volume, and W (g) is the weight of TCS used.

2.4. Statistical modeling of MB adsorption.

RSM is an essential tool for optimizing the adsorption process when several operational individual parameters and their mutual interactions affect the removal efficiency [42]. In this study, RSM was executed to examine the effects of three independent variables contact time (X_1), MB dye concentration (X_2), and TCS dose (X_3), on the MB removal efficiency onto TCS. The establishment of an experimental adsorption design was established using BBD implemented in design-expert software (version 8.0.1). All experiments were carried out at 21 ± °C and pH (MB) = 5.4. A three-factor and level (–α, –1, 0, 1, and α) consisting of 23 experiences were designed to optimize MB dye desorption. The ranges of the considered variables as well as the corresponding observed responses are summarized in Table 1. The numerical expression of the polynomial statistical model is formalized as follows [43,44]:

$$Y(\%) = \alpha_0 + \sum_{I=1}^{3} \alpha_i X_i + \sum_{I=1}^{3} \alpha_{ii} {X_i}^2 + \sum_{I<j} \alpha_{ij} X_i X_j \quad (4)$$

where Y (%) represents MB dye removal efficiency as a response; X_i and X_j are the selected independent variables; α_0 (intercept), α_i (linear effect), α_{ii} (quadratic effect), and α_{ij} (interaction effect) are the values of model coefficients. The values of the regression parameters such as the correlation coefficient r^2, adjusted r^2, F-value, and p-value (probability) were calculated using variance analysis (ANOVA) and used to determine the relevance and suitability of the predicated model. Based on the 95 % confidence level in the developed model, the significance of independent variables on the MB adsorption process was evaluated.

Table 1. Codes and variables of BBD matrix and experimental data for MB removal efficiency.

N° experience	Contact time		MB dye concentration		TCS dose		Removal (%)
	X_1	x_1	X_2	x_2	X_3	x_3	
1	-1	30	-1	200	-1	0.80	51.08
2	1	60	-1	200	-1	0.80	67.61
3	-1	30	1	400	-1	0.80	26.01
4	1	60	1	400	-1	0.80	36.30
5	-1	30	-1	200	1	1.80	87.17
6	1	60	-1	200	1	1.80	86.83

N° experience	Contact time		MB dye concentration		TCS dose		Removal (%)
	X_1	x_1	X_2	x_2	X_3	x_3	
7	-1	30	1	400	1	1.80	64.41
8	1	60	1	400	1	1.80	69.19
9	-α	20	0	300	0	1.30	62.51
10	-α	70	0	300	0	1.30	75.82
11	0	45	-α	132	0	1.30	81.92
12	0	45	+α	468	0	1.30	43.82
13	0	45	0	300	-α	0.46	29.45
14	0	45	0	300	+α	2.14	82.68
15	0	45	0	300	0	1.30	58.69
16	0	45	0	300	0	1.30	54.27
17	0	45	0	300	0	1.30	58.84
18	0	45	0	300	0	1.30	55.86
19	0	45	0	300	0	1.30	57.41
20	0	45	0	300	0	1.30	59.14
21	0	45	0	300	0	1.30	56.13
22	0	45	0	300	0	1.30	59.03
23	0	45	0	300	0	1.30	55.78

3. Results and Discussion

3.1. FTIR and SEM analysis.

The adsorption capacity of MB depends on the porosity and the chemical reactivity of functional groups present at the surface of TCS.

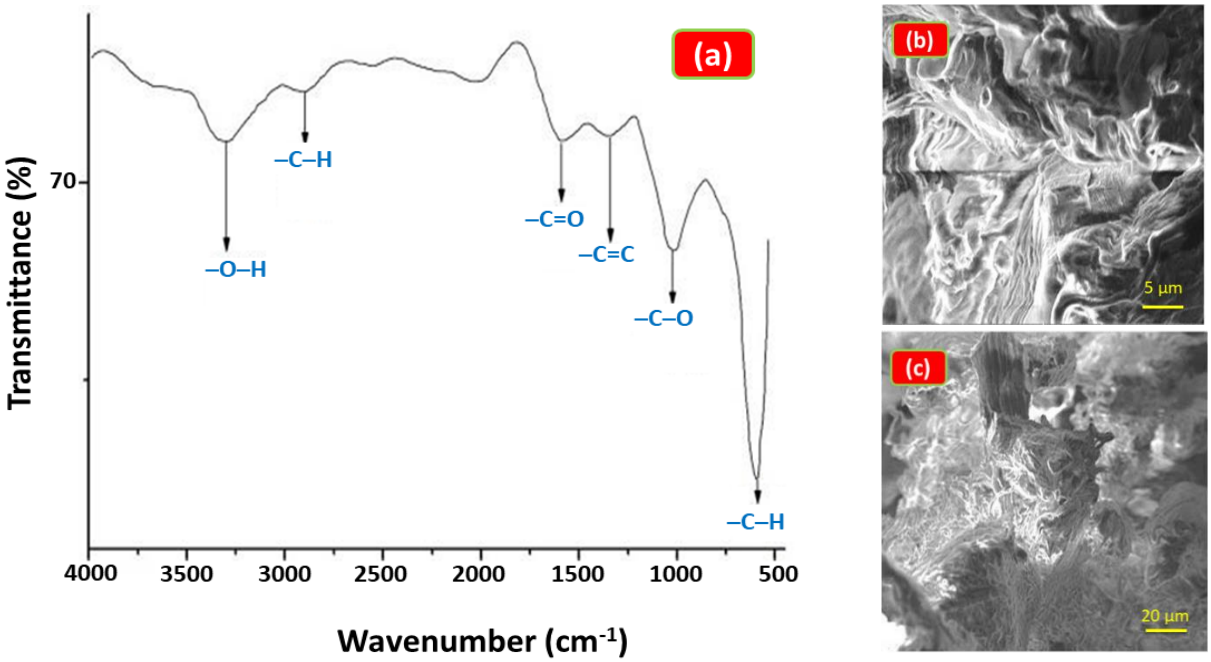

Figure 1. (**a**) FTIR and (**b,c**) SEM images of TCS.

The spectrum FTIR of TCS is shown in Figure 1a, the bond at 3326 cm^{-1} corresponds to hydroxyl –O–H stretching vibration of cellulose hemicelluloses and lignin [45,46], the small

strength band at approximately 2916 cm^{-1} is attributed to –C–H stretching [28,47], and the bands at 1608 cm^{-1}, 1316 cm^{-1}, and 1023 cm^{-1} represent stretching vibrations of –C=O of esters and acids [48,49], aromatic –C=C [18], and aliphatic –C–O stretching [50–52], respectively. Finally, the strong peak at 642 cm^{-1}corresponds to cellulose's –C–H deformation [53]. SEM images analyzed the morphology of TCS. Figures 1b and c show the surface texture and porosity of TCS. The TCS has a heterogeneous surface and is porous, as seen from its surface micrographs.

3.2. Adsorption study.

3.2.1. Effect of TCS dose.

The adsorption of MB onto TCS was studied by varying the adsorbent quantity (0.4–2.4 g L^{-1}) in solution while keeping the initial dye concentration (100 mg L^{-1}), temperature (21± 1 °C), and pH (5.4) constant for 120 min of contact time. As Figure 2a shows, MB removal increases from 38.39 to 86.54 % by increasing the adsorbent dosage from 0.4 to 1.8 g L^{-1}. Results imply that the number of active adsorption sites for MB adsorption corresponds to the applied dose, prompting higher removal efficiency [54]. After equilibrium between the adsorbent and dye in the solution, the removal percentage remains consistent at higher doses (>1.8 g L^{-1}) due to the saturation of active adsorption sites on the surface of TCS [55]. The optimum adsorbent dosage was considered o f 1.8 g L^{-1} to reach maximum MB removal efficiency.

3.2.2. Effect of contact time.

The batch adsorption experiments were conducted at different contact times (0 to 120 min) for an initial concentration of 100 mg L^{-1} of MB and 1.8 g L^{-1} of TCS dosage at pH=5.4 and temperature of 21 °C. As shown in Figure 2b, the MB adsorption on TCS was fast at first (until 60 min), but it declined. It may be attributed to many sites accessible on the surface of the adsorbent in the initial stage [56]. Then, with a decrease in several active sites, the adsorption rate became consistent [57]. Experimental data showed that equilibrium was achieved in 60 min with 49.05 mg g^{-1} adsorption capacity of MB.

3.2.3. Effect of MB dye concentration.

The experimental results for the adsorption properties of MB onto TCS at initial concentrations varied from 100 to 500 mg L^{-1} with keeping all other parameters consistent (TCS dose=1.8 g L^{-1}, temperature=21 ± 1 °C, contact time=60 min, and pH (MB)=5.4) are shown in Figure 2c. As illustrated in Figure 2c, by increasing MB concentration from100 to 400 mg L^{-1}, the adsorption capacity progressively increased from 44.25 to 120.49 mg g^{-1}; this increases due to available sites on the surface of TCS [58]. After 400 mg L^{-1}, we note the adsorption capacity of MB decreased due to active sites still being available, and no saturation occurred [59], also due to the increased competition among MB molecules for occupying available active sites.

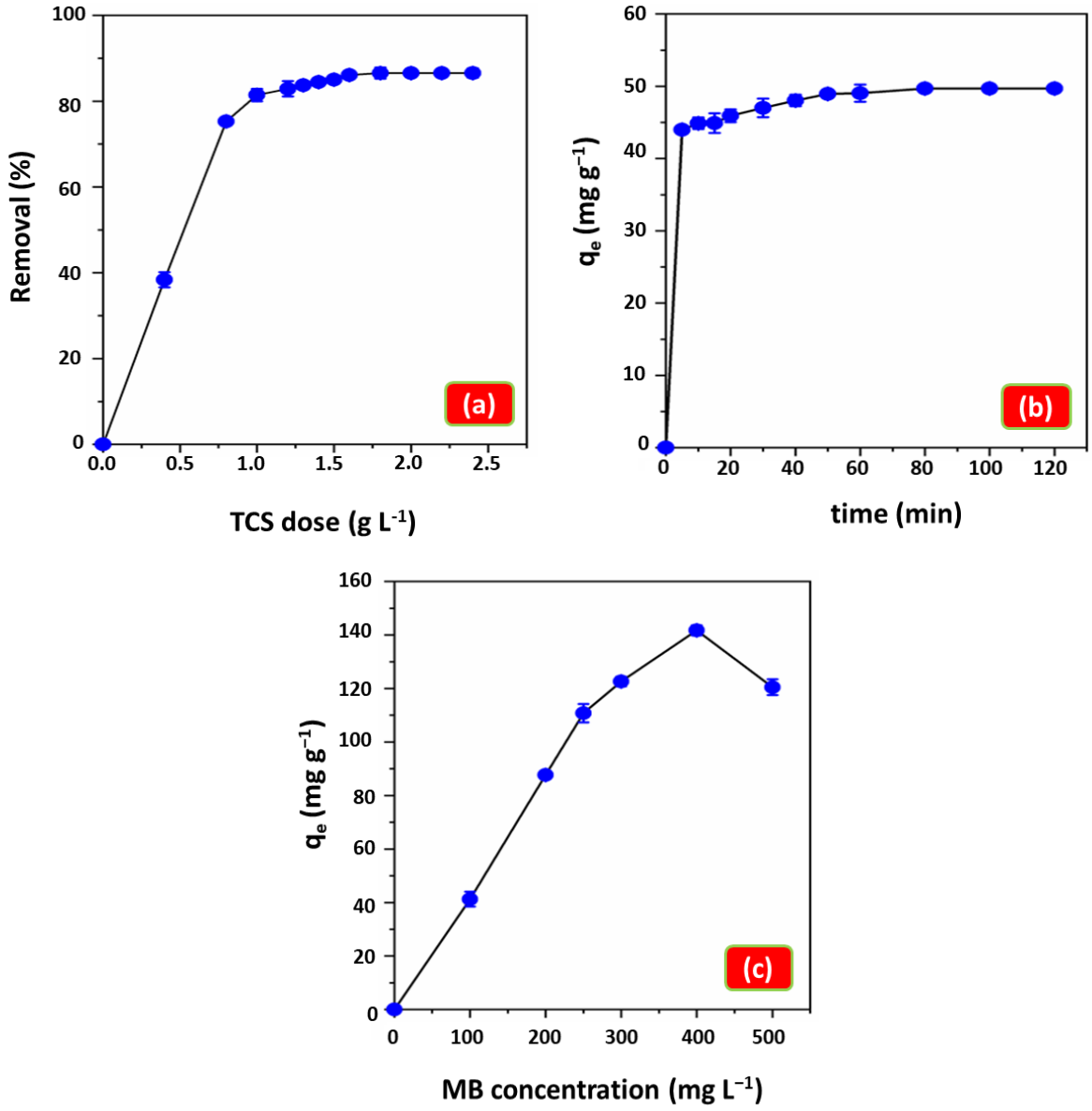

Figure 2. Effects of (**a**) TCS dose; (**b**) contact time; (**c**) dye concentration on MB adsorption using TCS.

3.3. Statistical optimization of MB adsorption.

3.3.1. Effect of TCS dose Analysis of variance (ANOVA).

Analysis of variance allows us to see whether the variables used for modeling have taken as a whole a significant effect on the response. The results of the analysis of variance are grouped in Table 2. F-value =152.2 is greater than that theoretical $F_{0.001}$ (9.13) = 6.98. The regression is significant at a confidence level of about 99 %. We see that the mathematical models for all responses are validated from the statistical test results: p-value < 1% and r^2, adjusted r^2 close to 1 [60]. The equation of the second-order polynomial model between tested factors and the MB dye removal (response) was obtained and described in the following Equation (5):

$$Y(\%) = 55.28 + 3.93X_1 - 11.73X_2 + 15.82X_3 + 3.81{X_1}^2 + 1.58{X_2}^2 - 2.79X_{13} + 1.99X_{23} \quad (5)$$

where Y (%) is the MB removal, X_1 is the contact time, X_2 is the MB concentration, X_3 is the TCS dose, $X_1^2 = X_1*X_1$, $X_2^2 = X_2*X_2$, X_{13} is the interaction between contact time and TCS dose, and X_{23} is the interaction between MB concentration and TCS dose.

Table 2. Analysis of variance (ANOVA) of surface response for MB adsorption on TCS.

Source	Sum of square	Degree of freedom	Mean square	F-value	p-value	r^2	Adjusted r^2
Regression	5901.16	9	655.68	152.2	<0.01	0.992	0.984
Residues	56	13	4.30				
Total	5957.16	22					

3.3.2. Signification and effects of different factors.

The purpose of this statistical test is to find out if any coefficients are not influential, that is, that do not affect each of the responses. If one or more coefficients do not influence all the responses, they can be removed from the mathematical model to simplify it and improve its quality. The estimated values of the model coefficients and the sings are given in Table 3. This table brings together the different factors and their meanings, and we notice that that the coefficients α_{33} (TCS dose*TCS dose) and α_{12} the interaction (contact time*MB dye concentration) are not influential on the quantity adsorbed since the significance value for these coefficients is greater than 5 % [61].

Table 3. Analysis of coefficients.

Coefficient	Degrees of freedom	t_{exp}	Signification (%)
α_0	57.28	-	82.85
α_1	3.93	1	6.99
α_2	-11.78	1	-20.97
α_3	15.82	1	28.18
α_{11}	3.81	1	7.32
α_{22}	1.58	1	3.04
α_{33}	-0.82	1	-1.58
α_{12}	-0.14	1	-0.19
α_{13}	-2.79	1	-3.81
α_{23}	1.99	1	2.72

3.3.3. Model validity.

Validating the model ensures that the experimental points' calculated responses are roughly the same as the measured responses. Table 4 collates the experimental results and the calculated results. The comparison between these two results shows that we have an excellent estimate of the model. It can therefore be adapted for interpretation of tests and for drawing up graphs. By plotting the parity curves giving the calculated responses as a function of the experimental responses (Figure 3), it can be seen that the model correlates the experimental results well.

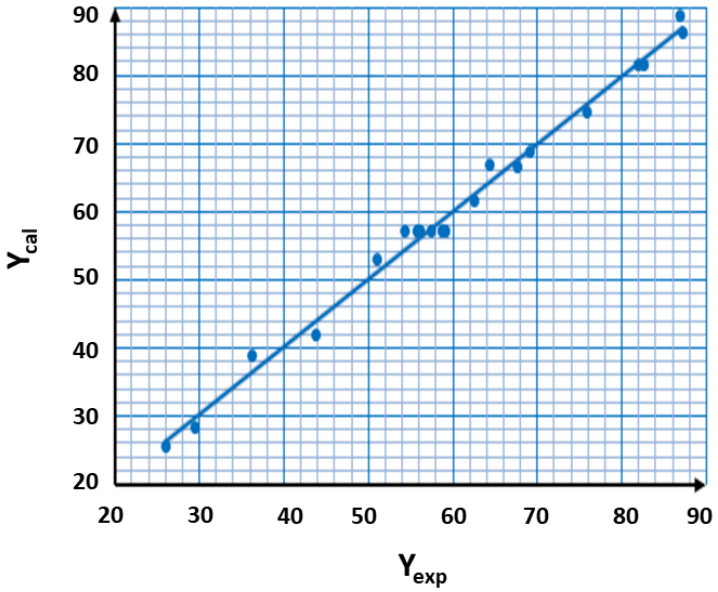

Figure 3. Y_{cal} as a function Y_{exp}.

Table 4. Comparison between experimental results and the values calculated responses from the model.

N° experience	Y_{exp}	Y_{cal}	Difference
1	51.08	52.94	-1.86
2	67.61	66.67	0.94
3	26.01	25.67	0.34
4	36.30	38.84	-2.54
5	87.17	86.19	0.98
6	86.83	88.73	-1.90
7	64.41	66.91	-2.5
8	69.19	68.89	0.23
9	62.51	61.54	1.05
10	75.82	74.66	1.15
11	81.92	81.57	0.34
12	43.82	41.95	1.86
13	29.45	28.34	1.10
14	82.68	81.57	1.01
15	58.69	57.28	1.41
16	54.27	57.28	-3.01
17	58.84	57.28	1.56
18	55.86	57.28	-1.43
19	57.41	57.28	0.13
20	59.14	57.28	1.85
21	56.13	57.28	-1.15
22	59.05	57.28	1.77
23	55.78	57.28	-1.50

3.3.4. Graphic study of residues.

To confirm that the model accurately describes variations in responses, care must be taken to ensure that local residues are not abnormally high. Figure 4 represents the change in average probability based on residues. The residues appear to be distributed generally in a straight line, proving that the values obtained are regular, symmetrical, and have no abnormal or aberrant values.

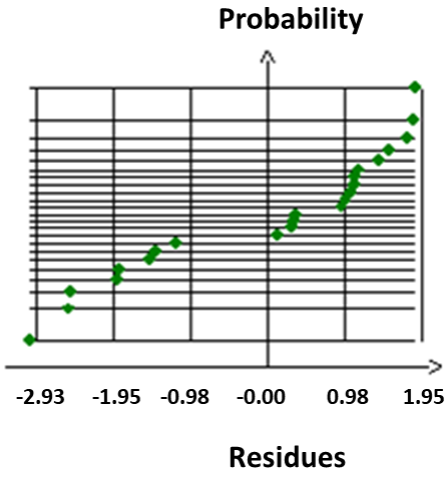

Figure 4. Line of Henry.

3.3.5. Validation of the model on internal test points.

This operation aims to validate the model on points far from the issues of the experiment matrix. The test points make it possible to verify that the polynomial model represents the variation of response in all domain points. The four points proposed by the software, the values calculated by the model, and the response experience on these four points are given in Table 5. It can be noted that the model makes it possible to correctly represent the variation of the responses in all topics of the domain since the differences between the experimental values and the values calculated by the model are considered to be small [62].

Table 5. Internal test points proposed by the software.

Tests	Variables			Removal		Difference (%)
	Contact time (min)	Concentration (mg L^{-1})	TCS dose (g L^{-1})	Model	Experience	
1	34	259	1.16	55.79	56.41	-0.62
2	56	259	1.16	60.25	63.02	-2.77
3	45	382	1.16	43.67	43.52	0.15
4	45	300	1.74	70.98	70.42	0.56

3.3.6. Graphical analysis of results.

Since the variation of three factors defines the experimental domain, the graphical analysis can be used to study the effects of these three variables on the response. The effect of the contact time, MB dye concentration, and TCS dose input factors on the response are given by three-dimensional graphs called response surfaces. The horizontal plane of the figure materializes the domain of variation of the three variables; the vertical axis materializes the variation of the removal. 2D and 3D surface response plots and response surfaces provide a

simple method for optimizing MB adsorption and identifying interactions between variables (Figure 5a, b, and c).

Each curve represents, in our case, an infinity of combinations between two variables when the other variables are kept at a constant level. Figures 5a and c confirm what we have already seen in Table 3, namely a positive effect of time on the response, which generally translates into an increase in efficiency when the contact time is increased [63].

Figures 5b and c show a positive effect of the TCS dose on the response, increasing efficiency when the TCS dose increases. We can also see from Figures 5b and c that the MB removal is significantly at low MB dye concentration than at high MB dye concentration. We can also observe, due to the increase in the concentration to reinforce the positive effect of the mass, what can be due according to Table 3 to the effect of the interaction TCS dose*concentration with a positive sign.

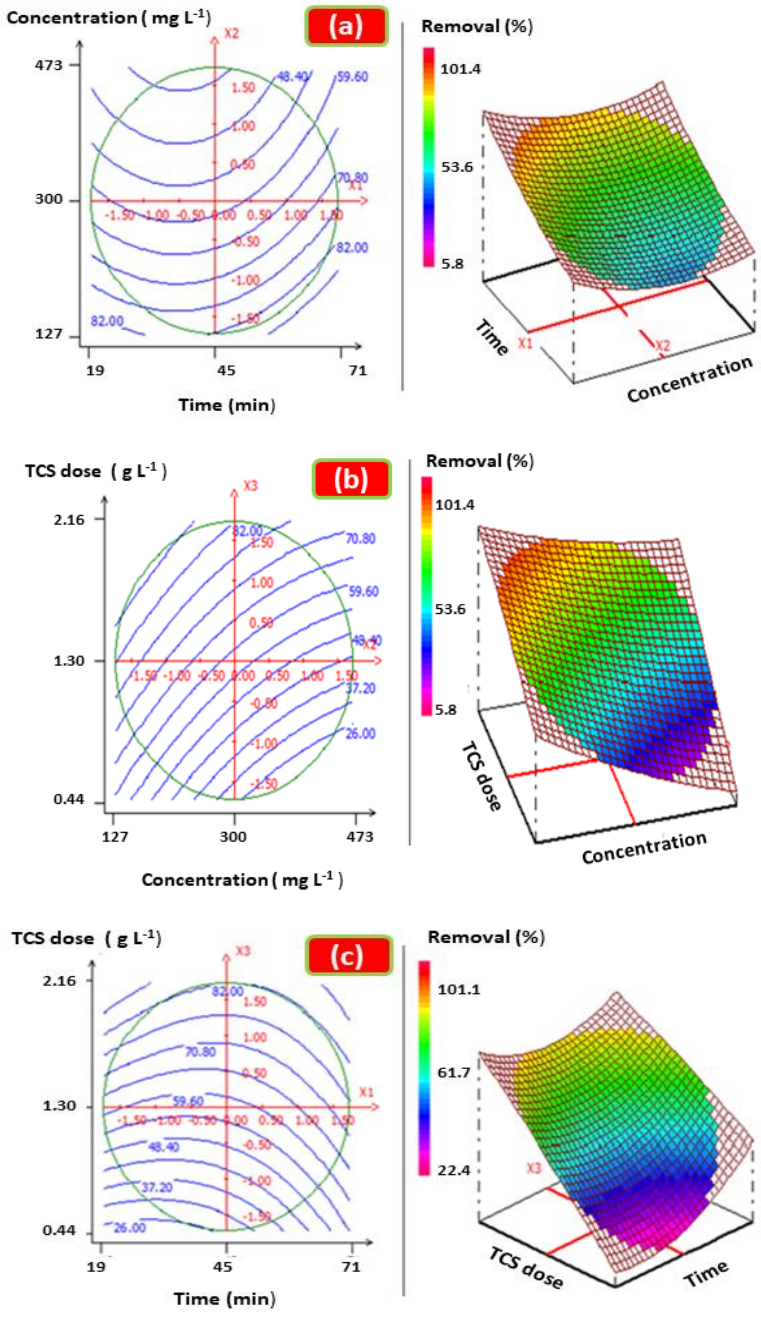

Figure 5. 2D and 3D surface response plots of MB removal on TCS: (**a**) MB concentration combined with contact time; (**b**) MB concentration combined with TCS dose; (**c**)TCS dose combined with contact time.

3.3.7. Individual and global desirability functions

The transformation of a particular value of a modeled response into a satisfaction index is graphically illustrated in Figure 6. This figure represents the desirability function D_1 of response Y_1. We have specified 29.45 as the minimum accepted value for the Y_1 response.

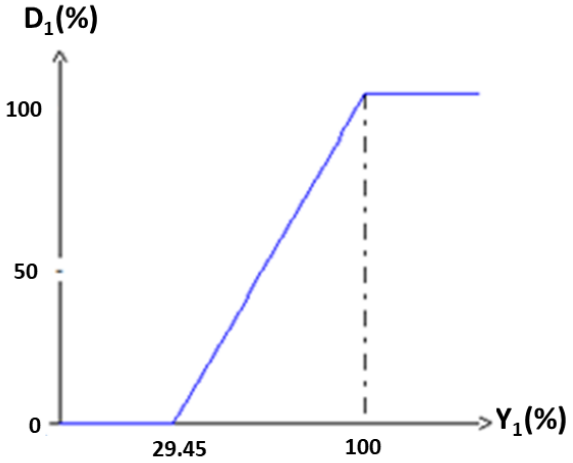

Figure 6. Individual desirability functions.

After transforming the response into individual desirability functions, defining an objective criterion that we will seek to optimize is necessary. The value of the global desirability function is defined from the geometric mean of the values of the individual desirability functions. It is also possible to give weight to the different responses. In this case, we obtain:

$$D = ({D_1}^{weight})^{1/weight} = D_1 \quad (6)$$

The aim is to search for a multi-criteria optimum obtained by a maximum value of the global desirability function D.

3.3.8. Multi-criteria optimum search.

The search for multi-criteria optimum consists of finding the level of factors that maximizes the value of the global desirability function. By default, this point is the center of the domain (contact time=45 min, MB dye concentration=300 mg L^{-1}, and TCS dose=1.3 g L^{-1}). After several calculations, the software displays the coordinates of the optimum found, and for each response, we obtain:

- ✓ Its value calculated at the optimum point;
- ✓ The value of the associated desirability function D_1;
- ✓ The weight of the response;
- ✓ The value of the global desirability function;

All the results of the multi-criteria optimization are given in Table 6. We obtained a high percentage of desirability for the Y_1 response (D_1=85.79 %). The value of this response calculated by the model is 89.48 % [64].

Table 6. Search result for the optimum.

Variable	Value
X_1	0.737
X_2	-1.242
X_3	0.956
Contac time (min)	56
MB concentration (mg L^{-1})	176

Variable	Value
TCS dose (g L^{-1})	1.78
Removal (%)	89.48
D_1 (%)	85.79
Desirability (%)	85.79
Weight	1

We calculated the removal with the optimal values of contact time (56 min), MB concentration (176 mg L^{-1}), and TCS dose (1.78 g L^{-1}). The response calculated by the model and obtained by experience is given in Table 7. The value of the yield calculated by the experiment is very close to that predicted by the experiment plan (difference of the order of 0.75). The results show the effectiveness of the experimental designs since we obtained a relatively high removal of 89 % [65].

Table 7. Comparison between the experiment and the solution found by the software.

	Contac time (min)	MB concentration (mg L^{-1})	TCS dose (g L^{-1})	Removal (%)	Difference (%)
Software	56	176	1.78	89.48	0.75
Experience	56	176	1.78	88.73	

3.4. Proposed adsorption mechanism.

The adsorption mechanism of MB onto the surface of TCS is proposed based on FTIR analysis is presented in Figure 7. From this figure, the methylene blue adsorption onto adsorbent is only interactions such as hydrogen bonding and electrostatic interaction between the MB dye molecules and surface TCS [66–68].

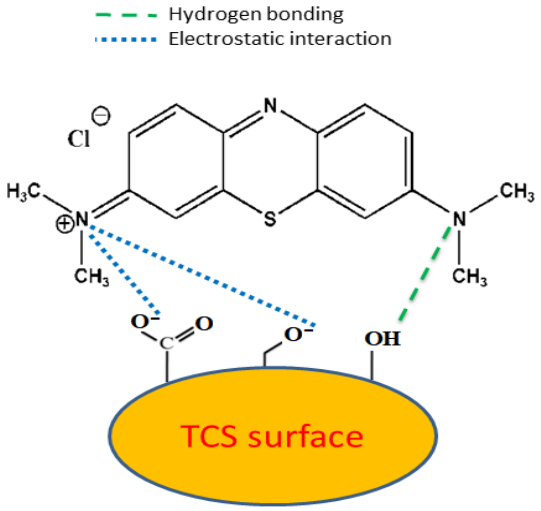

Figure 7. Proposed adsorption mechanism of MB onto TCS.

3.5. Regeneration of TCS.

The TCS was regenerated using 0.1 M HCl and reused in six consecutive adsorption-desorption for MB removal from aqueous solution in optimal conditions (TCS dose = 1.8 g L^{-1}, C_0=100 mg L^{-1}, pH=5.4, t=60 min, T=21 ± 1 °C). The results are illustrated in Figure 8. Further, experimental results showed that the dye adsorption efficiency of MB was gradually decreased from 88.31 to 82.25 % for six cycles. This decrease was attributed to the occupation of available sites on the TCS surface [69]. The regeneration and reusability of the tunics of corm saffron were compared with the previous study and listed in Table 8.

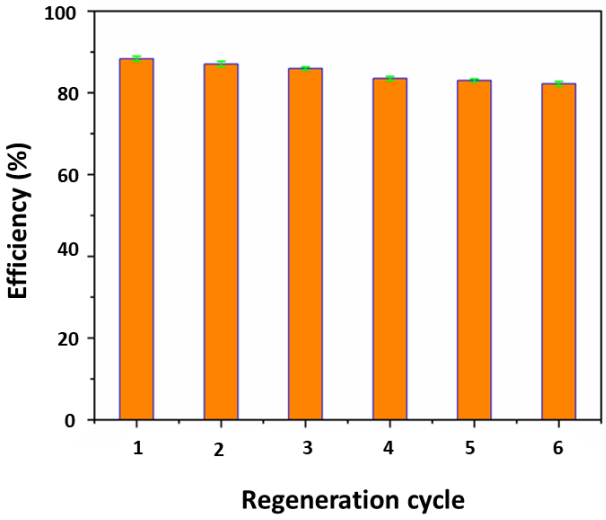

Figure 8. Regeneration of TCS for the removal of MB.

Table 8. Comparison of regeneration of some adsorbents for the MB removal.

Adsorbent	**Removal (%)**	**N° Cycle**	**Eluent**	**Refs.**
TCS	82.25	6	0.1 M HCl	This study
Salvinia minima	87.72	3	0.1 M HCl	[70]
Sepia shells	86.55	4	0.5 M HCl	[71]
Seeds of *Punica granatum L.*	79.00	2	CH_3COOH	[72]
Carboxylation kapok fiber	47.30	10	0.1 M HCl	[73]
Mandarin Peel	86.12	3	1 M HCl	[37]
Acid modified-Hazelnut shell	90.00	5	0.5 M HCl	[74]
bentonite coating (*Paintosorp*™)	92.60	3	C_2H_5OH	[75]
Natural clay	90.57	5	0.3 M HNO_3	[11]
Cellulose	98.20	4	0.1 M HCl	[76]
Leaves of Platanus	68.00	3	Deionized water	[33]

4. Conclusions

With Optimization of MB adsorption on tunics corm saffron from aqueous solution using Box-Behnken design (BBD) combined with response surface methodology (RSM) modeling. The influence of the three parameters such as TCS dose, contact time, MB dye concentration on adsorption of MB on TCS was studied. The results show that the application of the experimental design methodology makes it possible to correctly describe and model the influence of these three experimental parameters on MB adsorption efficiency. The highest MB removal efficiency (89.48 %) was achieved at values: contact time=56 min, MB dye concentration=176 mg L^{-1}, TCS dose=1.78 g L^{-1}. The regeneration study demonstrated that the TCS exhibited excellent reusability for MB dye removal from aqueous solutions. The above result further indicated that the TCS could be reused to remove highly efficient organic dyes from wastewaters.

Funding

This research received no external funding.

Acknowledgments

The authors declare no acknowledgments.

Conflicts of Interest

The authors declare no conflict of interest.

References

1. Smith, Y.R.; Bhattacharyya, D.; Willhard, T.; Misra, M. Adsorption of aqueous rare earth elements using carbon black derived from recycled tires. *Chem. Eng. J.* **2016**, *296*, 102–111, https://doi.org/10.1016/j.cej.2016.03.082.
2. Zhou, Y.; Lu, J.; Zhou, Y.; Liu, Y. Recent advances for dyes removal using novel adsorbents: A review. *Environ. Pollut.* **2019**, *252*, 352–365, https://doi.org/10.1016/J.ENVPOL.2019.05.072.
3. González, J.A.; Villanueva, M.E.; Piehl, L.L.; Copello, G.J. Development of a chitin/graphene oxide hybrid composite for the removal of pollutant dyes: Adsorption and desorption study. *Chem. Eng. J.* **2015**, *280*, 41–48, https://doi.org/10.1016/j.cej.2015.05.112.
4. Ip, A.W.M.; Barford, J.P.; McKay, G. Reactive Black dye adsorption/desorption onto different adsorbents: Effect of salt, surface chemistry, pore size and surface area. *J. Colloid Interface Sci.* **2009**, *337*, 32–38, https://doi.org/10.1016/j.jcis.2009.05.015.
5. Mittal, A.; Mittal, J.; Malviya, A.; Gupta, V.K. Adsorptive removal of hazardous anionic dye "Congo red" from wastewater using waste materials and recovery by desorption. *J. Colloid Interface Sci.* **2009**, *340*, 16–26, https://doi.org/10.1016/j.jcis.2009.08.019.
6. El Messaoudi, N.; El Khomri, M.; Dbik, A.; Bentahar, S.; Lacherai, A.; Bakiz, B. Biosorption of Congo red in a fixed-bed column from aqueous solution using jujube shell: Experimental and mathematical modeling. *J. Environ. Chem. Eng.* **2016**, *4*, 3848–3855, https://doi.org/10.1016/j.jece.2016.08.027.
7. El Messaoudi, N.; El Khomri, M.; Chlif, N.; Chegini, Z.G.; Dbik, A.; Bentahar, S.; Lacherai, A. Desorption of Congo red from dye-loaded Phoenix dactylifera date stones and Ziziphus lotus jujube shells. *Groundw. Sustain. Dev.* **2021**, *12*, 100552, https://doi.org/10.1016/j.gsd.2021.100552.
8. Afroze, S.; Sen, T.K.; Ang, M.; Nishioka, H. Adsorption of methylene blue dye from aqueous solution by novel biomass Eucalyptus sheathiana bark: equilibrium, kinetics, thermodynamics and mechanism. *Desalin. Water Treat.* **2016**, *57*, 5858–5878, https://doi.org/10.1080/19443994.2015.1004115.
9. Azzaz, A.A.; Jellali, S.; Assadi, A.A.; Bousselmi, L. Chemical treatment of orange tree sawdust for a cationic dye enhancement removal from aqueous solutions: kinetic, equilibrium and thermodynamic studies. *Desalin. Water Treat.* **2016**, *57*, 22107–22119, https://doi.org/10.1080/19443994.2015.1103313.
10. Pandian, A.M.K.; Karthikeyan, C.; Rajasimman, M. Isotherm and kinetic studies on adsorption of malachite green using chemically synthesized silver nanoparticles. *Nanotechnol. Environ. Eng.* **2017**, *2*, 1–17, https://doi.org/10.1007/s41204-016-0013-4.
11. Bentahar, S.; Dbik, A.; Khomri, M.E.; El Messaoudi, N.; Lacherai, A. Removal of a cationic dye from aqueous solution by natural clay. *Groundw. Sustain. Dev.* **2018**, *6*, 255–262, https://doi.org/10.1016/j.gsd.2018.02.002.
12. Valarmathi, M.; Gomathi, A.; Manisankar, P. Enhanced sensing of anthraquinone dyes using multiwalled carbon nanotubes modified electrode. *Int. J. Environ. Anal. Chem.* **2013**, *93*, 349–363, https://doi.org/10.1080/03067319.2011.629348.
13. Sarıcı Özdemir, Ç. Equilibrium, kinetic, diffusion and thermodynamic applications for dye adsorption with pine cone. *Sep. Sci. Technol.* **2019**, *54*, 3046–3054, https://doi.org/10.1080/01496395.2019.1565769.
14. Adeogun, A.I. Removal of methylene blue dye from aqueous solution using activated charcoal modified manganese ferrite (AC-MnFe2O4): kinetics, isotherms, and thermodynamics studies. *Part. Sci. Technol.* **2020**, *38*, 756–767, https://doi.org/10.1080/02726351.2019.1626516.
15. El Messaoudi, N.; El Khomri, M.; Goodarzvand Chegini, Z.; Chlif, N.; Dbik, A.; Bentahar, S.; Iqbal, M.; Jada, A.; Lacherai, A. Desorption study and reusability of raw and H_2SO_4 modified jujube shells (*Zizyphus lotus*) for the methylene blue adsorption. *Int. J. Environ. Anal. Chem.* **2021**, 1–17, https://doi.org/10.1080/03067319.2021.1912338.
16. Russo, V.; Masiello, D.; Trifuoggi, M.; Di Serio, M.; Tesser, R. Design of an adsorption column for methylene blue abatement over silica: From batch to continuous modeling. *Chem. Eng. J.* **2016**, *302*, 287–295, https://doi.org/10.1016/j.cej.2016.05.020.
17. Ali, I.; Asim, M.; Khan, T.A. Low cost adsorbents for the removal of organic pollutants from wastewater. *J. Environ. Manage.* **2012**, *113*, 170–183.
18. El Messaoudi, N.; El Khomri, M.; Bentahar, S.; Dbik, A.; Lacherai, A.; Bakiz, B. Evaluation of performance of chemically treated date stones: Application for the removal of cationic dyes from aqueous solutions. *J. Taiwan Inst. Chem. Eng.* **2016**, *67*, 244–253, https://doi.org/10.1016/j.jtice.2016.07.024.

19. Akpomie, K.G.; Conradie, J. Banana peel as a biosorbent for the decontamination of water pollutants. A review. *Environ. Chem. Lett.* **2020**, *18*, 1085–1112.
20. Bentahar, S.; Dbik, A.; Khomri, M.E.; El Messaoudi, N.; Lacherai, A. Adsorption of methylene blue, crystal violet and congo red from binary and ternary systems with natural clay: Kinetic, isotherm, and thermodynamic. *J. Environ. Chem. Eng.* **2017**, *5*, 5921–5932, https://doi.org/10.1016/j.jece.2017.11.003.
21. Chandane, V.; Singh, V.K. Adsorption of safranin dye from aqueous solutions using a low-cost agro-waste material soybean hull. *Desalin. Water Treat.* **2016**, *57*, 4122–4134, https://doi.org/10.1080/19443994.2014.991758.
22. El Messaoudi, N.; El Khomri, M.; Chegini, Z.G.; Dbik, A.; Bentahar, S.; Iqbal, M.; Jada, A.; Lacherai, A. Desorption of crystal violet from alkali-treated agricultural material waste: an experimental study, kinetic, equilibrium and thermodynamic modeling. *Pigment & Resin Technol.* **2021**, *ahead-of-print*, https://doi.org/10.1108/PRT-02-2021-0019.
23. Ashrafi, S.D.; Kamani, H.; Jaafari, J.; Mahvi, A.H. Experimental design and response surface modeling for optimization of fluoroquinolone removal from aqueous solution by NaOH-modified rice husk. *Desalin. Water Treat.* **2016**, *57*, 16456–16465, https://doi.org/10.1080/19443994.2015.1080188.
24. Dbik, A.; Bentahar, S.; El Khomri, M.; El Messaoudi, N.; Lacherai, A. Adsorption of Congo red dye from aqueous solutions using tunics of the corm of the saffron. In Proceedings of the Materials Today: Proceedings **2020**, 22.
25. Ghorbani, F.; Kamari, S.; Zamani, S.; Akbari, S.; Salehi, M. Optimization and modeling of aqueous Cr(VI) adsorption onto activated carbon prepared from sugar beet bagasse agricultural waste by application of response surface methodology. *Surfaces and Interfaces* **2020**, *18*, 100444, https://doi.org/10.1016/j.surfin.2020.100444.
26. El Messaoudi, N.; El Khomri, M.; Dabagh, A.; Chegini, Z.G.; Dbik, A.; Bentahar, S.; Lacherai, A.; Iqbal, M.; Jada, A.; Sher, F.; et al. Synthesis of a novel nanocomposite based on date stones/CuFe $_2$ O $_4$ nanoparticles for eliminating cationic and anionic dyes from aqueous solution. *Int. J. Environ. Stud.* **2021**, 1–19, https://doi.org/10.1080/00207233.2021.1929469.
27. Abbas, A.F.; Ahmed, M.J. Mesoporous activated carbon from date stones (Phoenix dactylifera L.) by one-step microwave assisted K2CO3 pyrolysis. *J. Water Process Eng.* **2016**, *9*, 201–207, https://doi.org/10.1016/j.jwpe.2016.01.004.
28. El Messaoudi, N.; Dbik, A.; El Khomri, M.; Sabour, A.; Bentahar, S.; Lacherai, A. Date stones of Phoenix dactylifera and jujube shells of Ziziphus lotus as potential biosorbents for anionic dye removal. *Int. J. Phytoremediation* **2017**, *19*, 1047–1052, https://doi.org/10.1080/15226514.2017.1319331.
29. El Messaoudi, N.; El Khomri, M.; Dbik, A.; Bentahar, S.; Lacherai, A. Selective and competitive removal of dyes from binary and ternary systems in aqueous solutions by pretreated jujube shell (Zizyphus lotus). *J. Dispers. Sci. Technol.* **2017**, *38*, 1168–1174, https://doi.org/10.1080/01932691.2016.1228070.
30. El Khomri, M.; El Messaoudi, N.; Dbik, A.; Bentahar, S.; Lacherai, A. Efficient adsorbent derived from Argania Spinosa for the adsorption of cationic dye: Kinetics, mechanism, isotherm and thermodynamic study. *Surfaces and Interfaces* **2020**, *20*, 100601, https://doi.org/10.1016/j.surfin.2020.100601.
31. da Silva, A.M.B.; Serrão, N.O.; de Gusmão Celestino, G.; Takeno, M.L.; Antunes, N.T.B.; Iglauer, S.; Manzato, L.; de Freitas, F.A.; Maia, P.J.S. Removal of rhodamine 6G from synthetic effluents using Clitoria fairchildiana pods as low-cost biosorbent. *Environ. Sci. Pollut. Res.* **2020**, *27*, 2868–2880, https://doi.org/10.1007/s11356-019-07114-6.
32. Rizzi, V.; D'Agostino, F.; Fini, P.; Semeraro, P.; Cosma, P. An interesting environmental friendly cleanup: The excellent potential of olive pomace for disperse blue adsorption/desorption from wastewater. *Dye. Pigment.* **2017**, *140*, 480–490, https://doi.org/10.1016/j.dyepig.2017.01.069.
33. Kong, L.; Gong, L.; Wang, J. Removal of methylene blue from wastewater using fallen leaves as an adsorbent. *Desalin. Water Treat.* **2015**, *53*, 2489–2500, https://doi.org/10.1080/19443994.2013.863738.
34. Uddin, M.K.; Nasar, A. Walnut shell powder as a low-cost adsorbent for methylene blue dye: isotherm, kinetics, thermodynamic, desorption and response surface methodology examinations. *Sci. Rep.* **2020**, *10*, 1–13, https://doi.org/10.1038/s41598-020-64745-3.
35. Al-Zoubi, H.; Zubair, M.; Manzar, M.S.; Manda, A.A.; Blaisi, N.I.; Qureshi, A.; Matani, A. Comparative Adsorption of Anionic Dyes (Eriochrome Black T and Congo Red) onto Jojoba Residues: Isotherm, Kinetics and Thermodynamic Studies. *Arab. J. Sci. Eng.* **2020**, *45*, 7275–7287, https://doi.org/10.1007/s13369-020-04418-5.
36. Kaur, R.; Kaur, H. Calotropis procera an effective adsorbent for removal of Congo red dye: isotherm and kinetics modelling. *Model. Earth Syst. Environ.* **2017**, *3*, 1–13, https://doi.org/10.1007/s40808-017-0274-3.
37. Unugul, T.; Nigiz, F.U. Preparation and Characterization an Active Carbon Adsorbent from Waste Mandarin Peel and Determination of Adsorption Behavior on Removal of Synthetic Dye Solutions. *Water. Air. Soil Pollut.* **2020**, *231*, 1–14.
38. Mondal, N.K.; Kar, S. Potentiality of banana peel for removal of Congo red dye from aqueous solution: isotherm, kinetics and thermodynamics studies. *Appl. Water Sci.* **2018**, *8*, 157, https://doi.org/10.1007/s13201-018-0811-x.
39. Filho, A.C.D.; Mazzocato, A.C.; Dotto, G.L.; Thue, P.S.; Pavan, F.A. Eragrostis plana Nees as a novel eco-

friendly adsorbent for removal of crystal violet from aqueous solutions. *Environ. Sci. Pollut. Res.* **2017**, *24*, 19909–19919, https://doi.org/10.1007/s11356-017-9365-y.
40. Asgher, M.; Bhatti, H.N. Removal of reactive blue 19 and reactive blue 49 textile dyes by citrus waste biomass from aqueous solution: Equilibrium and kinetic study. *Can. J. Chem. Eng.* **2012**, *90*, 412–419, https://doi.org/10.1002/cjce.20531.
41. Kumar, R.; Singh, V.; Devi, K.; Sharma, M.; Singh, M.K.; Ahuja, P.S. State of art of saffron (Crocus sativus L.) agronomy: A comprehensive review. *Food Rev. Int.* **2009**, *25*, 44–85, https://doi.org/10.1080/87559120802458503.
42. Pashaei, H.; Ghaemi, A.; Nasiri, M.; Karami, B. Experimental Modeling and Optimization of CO2 Absorption into Piperazine Solutions Using RSM-CCD Methodology. *ACS Omega* **2020**, *5*, 8432–8448, https://doi.org/10.1021/acsomega.9b03363.
43. Jawad, A.H.; Malek, N.N.A.; Abdulhameed, A.S.; Razuan, R. Synthesis of Magnetic Chitosan-Fly Ash/Fe3O4 Composite for Adsorption of Reactive Orange 16 Dye: Optimization by Box–Behnken Design. *J. Polym. Environ.* **2020**, *28*, 1068–1082, https://doi.org/10.1007/s10924-020-01669-z.
44. Zulfiqar, M.; Samsudin, M.F.R.; Sufian, S. Modelling and optimization of photocatalytic degradation of phenol via TiO2 nanoparticles: An insight into response surface methodology and artificial neural network. *J. Photochem. Photobiol. A Chem.* **2019**, *384*, 112039, https://doi.org/10.1016/j.jphotochem.2019.112039.
45. Salomón, Y.L. d. O.; Georgin, J.; Franco, D.S.P.; Netto, M.S.; Grassi, P.; Piccilli, D.G.A.; Oliveira, M.L.S.; Dotto, G.L. Powdered biosorbent from pecan pericarp (Carya illinoensis) as an efficient material to uptake methyl violet 2B from effluents in batch and column operations. *Adv. Powder Technol.* **2020**, *31*, 2843–2852, https://doi.org/10.1016/j.apt.2020.05.004.
46. Shakoor, S.; Nasar, A. Utilization of Cucumis Sativus Peel as an Eco-Friendly Biosorbent for the Confiscation of Crystal Violet Dye from Artificially Contaminated Wastewater . *Anal. Chem. Lett.* **2019**, *9*, 1–19, https://doi.org/10.1080/22297928.2019.1588162.
47. Siengchum, T.; Isenberg, M.; Chuang, S.S.C. Fast pyrolysis of coconut biomass - An FTIR study. *Fuel* **2013**, *105*, 559–565, https://doi.org/10.1016/j.fuel.2012.09.039.
48. Jawad, A.H.; Abdulhameed, A.S. Statistical modeling of methylene blue dye adsorption by high surface area mesoporous activated carbon from bamboo chip using KOH-assisted thermal activation. *Energy, Ecol. Environ.* **2020**, *5*, 456–469, https://doi.org/10.1007/s40974-020-00177-z.
49. Surip, S.N.; Abdulhameed, A.S.; Garba, Z.N.; Syed-Hassan, S.S.A.; Ismail, K.; Jawad, A.H. H2SO4-treated Malaysian low rank coal for methylene blue dye decolourization and cod reduction: Optimization of adsorption and mechanism study. *Surfaces and Interfaces* **2020**, *21*, 100641, https://doi.org/10.1016/j.surfin.2020.100641.
50. Feng, N.C.; Guo, X.Y. Characterization of adsorptive capacity and mechanisms on adsorption of copper, lead and zinc by modified orange peel. *Trans. Nonferrous Met. Soc. China (English Ed.* **2012**, *22*, 1224–1231, https://doi.org/10.1016/S1003-6326(11)61309-5.
51. Singh, J.; Ali, A.; Jaswal, V.S.; Prakash, V. Desalination of Cd2+ and Pb2+ from paint industrial wastewater by Aspergillus niger decomposed Citrus limetta peel powder. *Int. J. Environ. Sci. Technol.* **2015**, *12*, 2523–2532, https://doi.org/10.1007/s13762-014-0620-1.
52. Vargas, V.H.; Paveglio, R.R.; Pauletto, P. de S.; Salau, N.P.G.; Dotto, L.G. Sisal fiber as an alternative and cost-effective adsorbent for the removal of methylene blue and reactive black 5 dyes from aqueous solutions. *Chem. Eng. Commun.* **2020**, *207*, 523–536, https://doi.org/10.1080/00986445.2019.1605362.
53. Wakkel, M.; Khiari, B.; Zagrouba, F. Textile wastewater treatment by agro-industrial waste: Equilibrium modelling, thermodynamics and mass transfer mechanisms of cationic dyes adsorption onto low-cost lignocellulosic adsorbent. *J. Taiwan Inst. Chem. Eng.* **2019**, *96*, 439–452, https://doi.org/10.1016/j.jtice.2018.12.014.
54. Hoang, L.P.; Van, H.T.; Hang Nguyen, T.T.; Nguyen, V.Q.; Thang, P.Q. Coconut shell activated carbon/CoFe2O4 composite for the removal of rhodamine B from aqueous solution. *J. Chem.* **2020**, *2020*, https://doi.org/10.1155/2020/9187960.
55. Romdhane, D.F.; Satlaoui, Y.; Nasraoui, R.; Charef, A.; Azouzi, R. Adsorption, Modeling, Thermodynamic, and Kinetic Studies of Methyl Red Removal from Textile-Polluted Water Using Natural and Purified Organic Matter Rich Clays as Low-Cost Adsorbent. *J. Chem.* **2020**, *2020*, https://doi.org/10.1155/2020/4376173.
56. Rouhi, M.; Lakouraj, M.M.; Tashakkorian, H.; Hasantabar, V. Novel carbon based bioactive nanocomposites of aniline/indole copolymer for removal of cationic dyes from aqueous solution: Kinetics and isotherms. *New J. Chem.* **2019**, *43*, 2400–2410, https://doi.org/10.1039/c8nj02924e.
57. Aljeboree, A.M.; Alshirifi, A.N.; Alkaim, A.F. Kinetics and equilibrium study for the adsorption of textile dyes on coconut shell activated carbon. *Arab. J. Chem.* **2017**, *10*, S3381–S3393, https://doi.org/10.1016/j.arabjc.2014.01.020.
58. Al-Ghouti, M.A.; Khraisheh, M.A.M.; Ahmad, M.N.M.; Allen, S. Adsorption behaviour of methylene blue onto Jordanian diatomite: A kinetic study. *J. Hazard. Mater.* **2009**, *165*, 589–598, https://doi.org/10.1016/j.jhazmat.2008.10.018.
59. Jarrah, A.; Farhadi, S. Preparation and characterization of novel polyoxometalate/CoFe2O4/metal-organic framework magnetic core-shell nanocomposites for the rapid removal of organic dyes from water. *RSC Adv.*

2020, *10*, 39881–39893, https://doi.org/10.1039/d0ra04603e.
60. Bilici Baskan, M.; Pala, A. A statistical experiment design approach for arsenic removal by coagulation process using aluminum sulfate. *Desalination* **2010**, *254*, 42–48, https://doi.org/10.1016/j.desal.2009.12.016.
61. Yabalak, E.; Görmez, Ö.; Gizir, A.M. Subcritical water oxidation of propham by H2O2 using response surface methodology (RSM). *J. Environ. Sci. Heal. - Part B Pestic. Food Contam. Agric. Wastes* **2018**, *53*, 334–339, https://doi.org/10.1080/03601234.2018.1431468.
62. Chakraborty, D.; Gupta, G.; Kaur, B. Metabolic engineering of E. coli top 10 for production of vanillin through FA catabolic pathway and bioprocess optimization using RSM. *Protein Expr. Purif.* **2016**, *128*, 123–133, https://doi.org/10.1016/j.pep.2016.08.015.
63. Nitnithiphrut, P.; Pimsri, R.; Seithtanabutara, V. RSM optimization for the production of activated carbons from para-wood residue. In Proceedings of the Key Engineering Materials; Trans Tech Publications Ltd, 2017, *718*, 100–104.
64. Gupta, V.K.; Fakhri, A.; Rashidi, S.; Ibrahim, A.A.; Asif, M.; Agarwal, S. Optimization of toxic biological compound adsorption from aqueous solution onto Silicon and Silicon carbide nanoparticles through response surface methodology. *Mater. Sci. Eng. C* **2017**, *77*, 1128–1134, https://doi.org/10.1016/j.msec.2017.03.156.
65. Wan, Y.; Liu, X.; Liu, P.; Zhao, L.; Zou, W. Optimization adsorption of norfloxacin onto polydopamine microspheres from aqueous solution: Kinetic, equilibrium and adsorption mechanism studies. *Sci. Total Environ.* **2018**, *639*, 428–437, https://doi.org/10.1016/j.scitotenv.2018.05.171.
66. Dinh, V.P.; Huynh, T.D.T.; Le, H.M.; Nguyen, V.D.; Dao, V.A.; Hung, N.Q.; Tuyen, L.A.; Lee, S.; Yi, J.; Nguyen, T.D.; et al. Insight into the adsorption mechanisms of methylene blue and chromium(III) from aqueous solution onto pomelo fruit peel. *RSC Adv.* **2019**, *9*, 25847–25860, https://doi.org/10.1039/c9ra04296b.
67. Jawad, A.H.; Abdulhameed, A.S.; Mastuli, M.S. Acid-factionalized biomass material for methylene blue dye removal: a comprehensive adsorption and mechanism study. *J. Taibah Univ. Sci.* **2020**, *14*, 305–313, https://doi.org/10.1080/16583655.2020.1736767.
68. Bounaas, M.; Bouguettoucha, A.; Chebli, D.; Gatica, J.M.; Vidal, H. Role of the Wild Carob as Biosorbent and as Precursor of a New High-Surface-Area Activated Carbon for the Adsorption of Methylene Blue. *Arab. J. Sci. Eng.* **2021**, *46*, 325–341, https://doi.org/10.1007/s13369-020-04739-5.
69. Hu, X.; Yan, L.; Wang, Y.; Xu, M. Freeze-thaw as a route to build manageable polysaccharide cryogel for deep cleaning of crystal violet. *Chem. Eng. J.* **2020**, *396*, 125354, https://doi.org/10.1016/j.cej.2020.125354.
70. Pérez-Morales, J.M.; Sánchez-Galván, G.; Olguín, E.J. Continuous dye adsorption and desorption on an invasive macrophyte (Salvinia minima). *Environ. Sci. Pollut. Res.* **2019**, *26*, 5955–5970, https://doi.org/10.1007/s11356-018-04097-8.
71. Elgarahy, A.M.; Elwakeel, K.Z.; Elshoubaky, G.A.; Mohammad, S.H. Untapped Sepia Shell–Based Composite for the Sorption of Cationic and Anionic Dyes. *Water. Air. Soil Pollut.* **2019**, *230*, 1–23, https://doi.org/10.1007/s11270-019-4247-1.
72. Uddin, M.K.; Nasar, A. Decolorization of Basic Dyes Solution by Utilizing Fruit Seed Powder. *KSCE J. Civ. Eng.* **2020**, *24*, 345–355, https://doi.org/10.1007/s12205-020-0523-2.
73. Zhang, X.; Duan, C.; Jia, X.; Dai, B. Carboxylation kapok fiber as a low-cost, environmentally friendly adsorbent with remarkably enhanced adsorption capacity for cationic dyes. *Res. Chem. Intermed.* **2016**, *42*, 5069–5085, https://doi.org/10.1007/s11164-015-2345-2.
74. Lü, L.; Jiang, X.; Jia, L.; Ai, T.; Wu, H. Kinetic and thermodynamic studies on adsorption of Cu2+, Pb2+, methylene blue and malachite green from aqueous solution using AMPS-modified hazelnut shell powder. *Chem. Res. Chinese Univ.* **2017**, *33*, 112–118, https://doi.org/10.1007/s40242-017-6243-6.
75. Momina, M.; Shahadat, M.; Ismail, S. Regeneration Potential of Bentonite-Based Paintosorp™ for Removal of Industrial Dye. *Arab. J. Sci. Eng.* **2020**, *45*, 551–561, https://doi.org/10.1007/s13369-019-04275-x.
76. Jodeh, S.; Hamed, O.; Melhem, A.; Salghi, R.; Jodeh, D.; Azzaoui, K.; Benmassaoud, Y.; Murtada, K. Magnetic nanocellulose from olive industry solid waste for the effective removal of methylene blue from wastewater. *Environ. Sci. Pollut. Res.* **2018**, *25*, 22060–22074, https://doi.org/10.1007/s11356-018-2107-y.